A cross-species neural integration of gravity for motor optimization

Jeremie Gaveau, Sidney Grospretre, Bastien Berret, Dora Angelaki, Charalambos Papaxanthis

NEUROSCIENCE

A cross-species neural integration of gravity for motor optimization

Jeremie Gaveau[1,2]*, Sidney Grospretre[1,3], Bastien Berret[4,5,6], Dora E. Angelaki[7†], Charalambos Papaxanthis[1†]

Recent kinematic results, combined with model simulations, have provided support for the hypothesis that the human brain shapes motor patterns that use gravity effects to minimize muscle effort. Because many different muscular activation patterns can give rise to the same trajectory, here, we specifically investigate gravity-related movement properties by analyzing muscular activation patterns during single-degree-of-freedom arm movements in various directions. Using a well-known decomposition method of tonic and phasic electromyographic activities, we demonstrate that phasic electromyograms (EMGs) present systematic negative phases. This negativity reveals the optimal motor plan's neural signature, where the motor system harvests the mechanical effects of gravity to accelerate downward and decelerate upward movements, thereby saving muscle effort. We compare experimental findings in humans to monkeys, generalizing the Effort-optimization strategy across species.

INTRODUCTION

The ability to purposely move one's own body is a critical survival function that humans and animals master with apparent ease. However, even the most straightforward body limb movement entails inherent difficulties for which the motor system has evolved sophisticated solutions (*1*, *2*). One of these solutions is to learn internal models to disambiguate sensory information and predict forthcoming movement dynamics. On Earth, a pervasive component affecting perception and motion is gravity (*3*, *4*). Studies in both humans and nonhuman primates have provided strong evidence that the brain has an internal representation of gravity. This representation is thought to involve neural computations of the brain stem, the cerebellum, the vestibular cortex, and the anterior thalamus (*5*–*10*). Although the neural representation of gravity is well documented, how it may benefit the production of suitable motor commands is unclear. Yet, living organisms produce successful movements while facing gravity effects every day. It is critical to shed light on the neural computations that underpin motor planning and control in the gravity field.

When moving our body limbs, the brain generates neural commands that must consider both inertial forces and gravity forces. Functional segregation of inertial forces—related to the limb's velocity and acceleration—and gravity forces—related to the limb's position—was long assumed (*11*–*13*). According to this assumption, the internal model of gravity is used to compensate for the effects of gravity force throughout the entire movement. That is, neural commands produce a muscular force that is equal and opposite to the gravity force. Such a neural policy is thought to facilitate the production of accurate movements to changing directions, amplitudes, durations, and loads, by merely scaling the inertial-dependent part of the motor command. Albeit based on old literature, this influential compensation hypothesis still guides current research in various fields such as motor control (*14*, *15*), movement perception (*16*, *17*), or neuro-rehabilitation (*18*, *19*).

On the other hand, recent kinematic results challenged this prevalent theory by revealing velocity profiles for monoarticular arm movements whose temporal structure changes according to movement direction relative to the gravity vertical (*20*–*24*). This finding is straightforward because, during monoarticular movements, only the gravity force changes with movement direction; inertial forces are direction independent. Thus, this observation contradicts the fundamental premise of the compensation hypothesis, which assumes direction-invariant kinematics. In contrast, the reported direction-dependent kinematics of human single-joint rotations are consistent with an optimal control strategy that discounts muscle effort (*23*–*25*). Such an effort-optimization hypothesis assumes an internal model of gravity to take advantage of its effects rather than to compensate for them.

During adaptation to microgravity, the properties of arm movements further supported the effort-optimization hypothesis. As predicted by an optimization model, the direction dependence of arm movements progressively vanished in microgravity (*24*). This contrasts with the traditional compensation view that the brain uses internal models of perturbing forces for their compensation, such that stereotypic trajectories can be maintained (*11*, *12*, *26*). A more recent view is that motor adaptation constitutes a reoptimization process whereby newly constructed/calibrated internal models generate newly shaped trajectories (*24*, *27*, *28*).

Support for the effort-optimization hypothesis is so far limited to kinematic findings. This limitation is problematic because of the redundancy between the muscular and kinematic levels (*29*). Because many different muscular activation patterns can give rise to the same trajectory, using kinematic data exclusively to infer central processes is insufficient (*30*, *31*). Establishing that direction-dependent kinematics truly reflects motor commands that discount muscle effort requires additional evidence from muscle dynamics. Here, we analyze muscular activation patterns, in humans and monkeys, during single-degree-of-freedom arm movements performed in various directions. Although humans and monkeys are close relatives, significant structural differences exist between their brains and bodies. Here, we generalize the Effort-optimization strategy across species,

[1]INSERM U1093-CAPS, Université Bourgogne Franche-Comté, UFR des Sciences du Sport, F-21000 Dijon, France. [2]Department of Neuroscience, Baylor College of Medicine, Houston, TX 77030, USA. [3]EA4660-C3S Laboratory-Culture, Sport, Health and Society Univ. Bourgogne Franche-Comté, Besançon, France. [4]CIAMS, Université Paris-Saclay, Orsay, France. [5]CIAMS, Université d'Orléans, Orléans, France. [6]Institut Universitaire de France (IUF) , Paris, France. [7]New York University, New York City, NY 10003, USA.
*Corresponding author. Email: jeremie.gaveau@u-bourgogne.fr
†These authors contributed equally to this work.

thereby paving the way for neurophysiological studies of optimal motor control processes.

RESULTS

We trained three rhesus monkeys to perform earth-vertical and earth-horizontal arm movements around the shoulder joint (Fig. 1A). We also asked two groups of humans to perform earth-vertical and earth-horizontal arm movements from two different body orientations (seated upright and 90° tilted in roll). Arm movements were parallel to the participants' head/feet body axis in a first group (ego-parallel group, $n = 8$; Fig. 1B) and perpendicular to it in a second group (ego-perpendicular group, $n = 8$; Fig. 1C). A comparison between the ego-parallel group and the ego-perpendicular group allows dissociation of arm movement direction in body- and gravity-centered frames of reference.

Monkey and human arm movement kinematics follow similar direction-dependent asymmetries

Reaching arm movements typically exhibits bell-shaped velocity profiles (*32*). Velocity first rises to a peak (acceleration phase) and then declines back to zero (deceleration phase; see Fig. 2, A and B). As previously reported, single-degree-of-freedom human arm movements show direction-dependent asymmetries in the earth-vertical but not the earth-horizontal plane (*20*, *21*). A shorter and steeper acceleration profile for upward than for downward movements characterizes these direction-dependent asymmetries (rise to peak velocity in Fig. 2, A and B, top traces). Because previous work already demonstrated that this effect was independent of body orientation (*21*), Fig. 2 presents averaged results across both groups of humans. We found that monkeys also exhibit direction-dependent arm kinematics in the vertical plane only (Fig. 2, A and B, bottom traces). As in humans, the acceleration duration is shorter and steeper for upward than for downward movements. The peak acceleration (which quantifies the steepness of the acceleration phase) and the duration to peak velocity (which specifies the length of the acceleration phase) illustrate this result in Fig. 2 (C to F).

Direction-dependent asymmetry was further quantified using multiple parameters (fig. S1 and table S1). Although movement duration and amplitude were similar for all directions ($P > 0.19$ in all cases; see table S2 for all statistical comparisons), a significant main effect of direction was observed for peak acceleration, peak velocity, relative time to peak acceleration, and relative time to peak velocity ($P < 0.003$ in all cases). Post hoc comparisons, between opposite directions, yielded significant effects in the earth-vertical but not the earth-horizontal plane ($P < 0.02$ in all cases). Thus, kinematic asymmetries in monkeys are similar to those previously known in humans.

Figure 3 (A and B) depicts the kinematic predictions of the Smooth-Effort model in all directions. As previously reported and newly observed here in monkeys (*23*–*25*), taking advantage of gravity effects, to accelerate the arm downward and to decelerate the arm upward, predicts direction-dependent kinematics in the earth-vertical plane and direction-independent kinematics in the earth-horizontal plane. Instead, theoretical models compensating for gravity effects predict

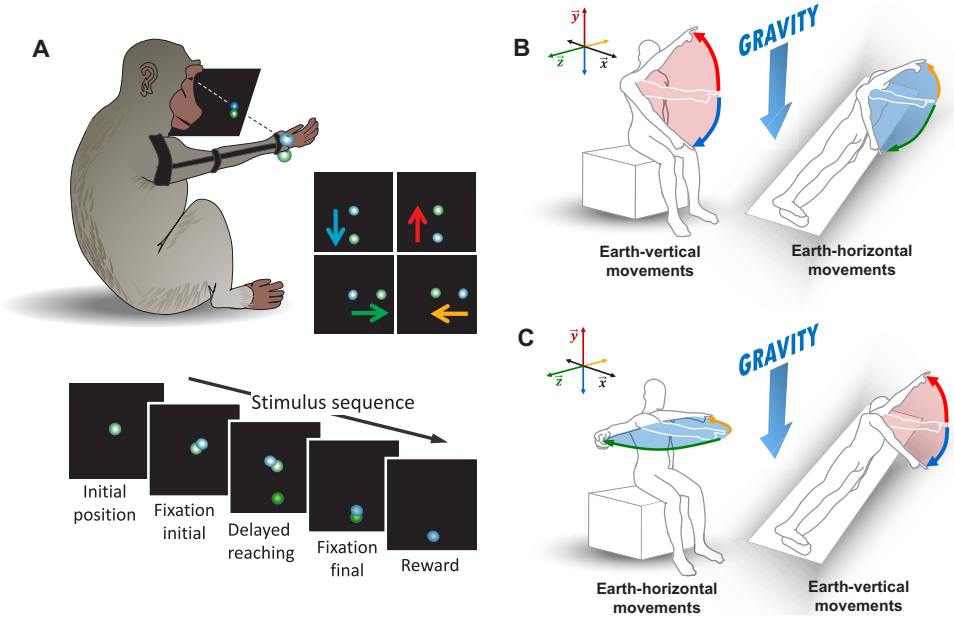

Fig. 1. Experimental setup. (**A**) Three monkeys performed monoarticular point-to-point arm movements between sets of two virtual targets. Positions of initial and final targets implied a leftward (yellow arrow), a rightward (green), a downward (blue), or an upward (red) movement. The monkeys performed a delayed reaching task with fixation periods on the initial and the final target (see stimulus sequence in lower part of the panel and Methods for details). (**B**) Ego-parallel group setup. Starting with their right arm perpendicular to the trunk, eight humans performed single-degree-of-freedom reaching arm movements between sets of two targets. Positions of targets implied movements toward the head (shoulder flexion) or the feet (shoulder extension), in the earth-vertical plane (participant seated, red/blue arrows) and in the earth-horizontal plane (participant reclined, yellow/green arrows), i.e., targets were rotated with the participant. (**C**) Ego-perpendicular group setup (eight humans). Same general organization as the first group but movements were perpendicular to the body axis (see Methods). In all three panels, *x*, *y*, and *z* axes illustrate the world coordinate system. For all figures, the color code is gravity centered, as follows: Red is against gravity (+y); blue is with gravity (−y); yellow is perpendicular to gravity, leftward (−z); green is rightward (+z).

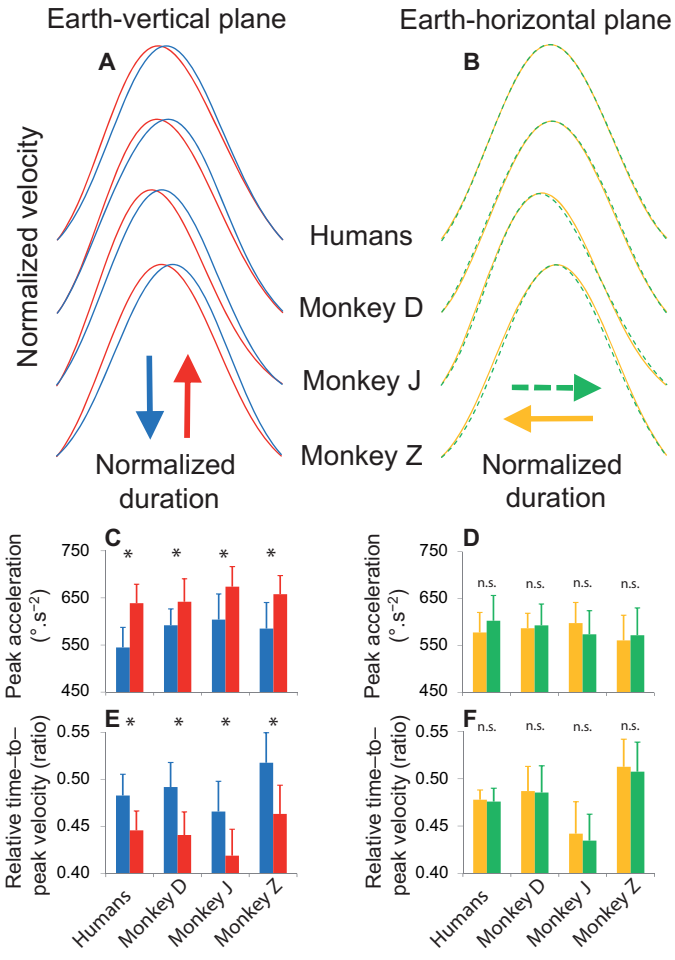

Fig. 2. Direction-dependent arm kinematics in monkeys and humans. Mean velocity profiles recorded in opposed directions in the earth-vertical (**A**) and the earth-horizontal plane (**B**) for each monkey and all humans ($n = 16$). Colored arrows indicate movement directions. Green profiles are dashed to better show the superposition on yellow profiles. Traces are amplitude and duration normalized to ease directional comparisons. Typical movement durations for monkeys and humans are detailed in table S1. Direction-dependent kinematics is observed in the earth-vertical plane but not in the earth-horizontal plane. The amplitude of the acceleration peak for each monkey and all humans ($n = 16$) is presented for opposed directions in the earth-vertical plane (**C**) and the earth-horizontal plane (**D**). n.s., not significant. The relative duration to peak velocity for each monkey and all humans ($n = 16$) is presented for opposed directions in the earth-vertical plane (**E**) and the earth-horizontal plane (**F**). Error bars represent the SD of the mean between recording sessions for each monkey and between participants for humans. *$P < 0.05$.

invariant kinematics both in the earth-vertical and in the earth horizontal planes (*23*–*25*). Figure S2 (A and B) depicts the kinematic predictions of the Minimum Jerk model (*33*), a model minimizing a kinematic cost and, therefore, adequately illustrating the compensation hypothesis.

Next, we examine muscular activation patterns to understand the production of direction-dependent arm kinematics further. Because of the redundancy between the muscular and kinematic levels (*29*), many different muscular activation patterns can give rise to the same velocity profile (*30*, *31*). Does the neural integration of gravity truly blossom into muscular activation patterns that discount muscle effort?

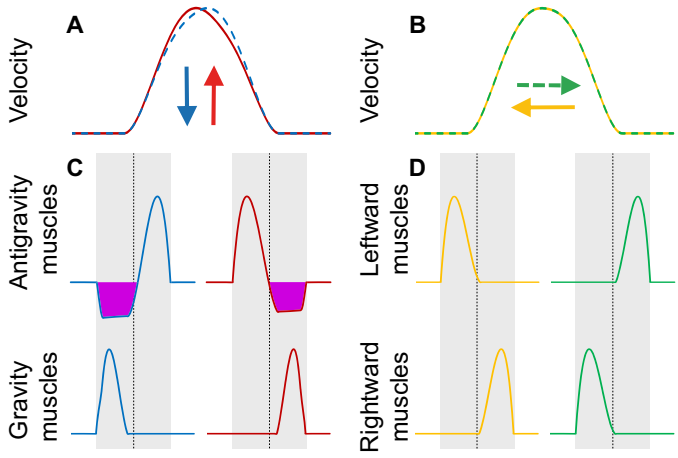

Fig. 3. Predictions of the Smooth-Effort model. The Smooth-Effort model simulates motor planning of arm movements that minimize a hybrid cost including both an effort and a kinematic component (*23*, *24*, *53*). Previous work has demonstrated that the production of directional asymmetries in the vertical plane is solely produced by the effort component of this hybrid cost (*24*). (**A**) Predicted velocity patterns in the vertical plane. (**B**) Predicted velocity patterns in the horizontal plane. (**C**) Phasic antigravity and gravity muscle patterns in the vertical plane. (**D**) Phasic rightward and leftward muscle patterns in the horizontal plane. The gray vertical areas denote movement duration, and the vertical dashed lines denotes 50% of movement duration. These simulations (20° movement amplitude in 400 ms) reveal that minimizing muscle effort requires deactivating antigravity muscles below the theoretical tonic level, therefore producing negative phasic patterns (purple areas). Hence, energetically efficient muscle and kinematic patterns are directionally asymmetric in the vertical plane but not in the horizontal plane. All profiles are normalized in duration and amplitude.

Phasic EMG activity supports the effort-optimization hypothesis

Two types of muscles can contribute to the arm's motion in the earth-vertical plane: those that pull against gravity (toward positive y axis in Fig. 1) and those that pull with gravity (toward negative y axis). Hereafter, the first type is named antigravity muscles, and the second type is named gravity muscles. In the earth-horizontal plane, to produce the arm motion, the muscles pull perpendicularly to gravity. Hereafter, the muscles pulling toward the positive z axis are named rightward muscles, and the opposite ones are named leftward muscles.

We applied a simple and widely used decomposition method to isolate the tonic (gravity-dependent force) and the phasic (inertial-dependent force) electromyogram (EMG) components from the full EMG signal (*13*, *15*, *34*–*37*). The tonic component emanates from the motionless rest periods before and after the movement (fig. S3, B and D). The phasic component results from the subtraction of the tonic activity from the total EMG (fig. S3, C to E). This subtraction stems from the compensation hypothesis, according to which the tonic component would compensate for the gravity force, whereas the phasic component would produce changes in arm velocity (*11*–*13*). Here, we take advantage of this method to test discriminant predictions of the Compensation and the Effort-optimization hypotheses.

The effort-optimization hypothesis predicts phasic components of antigravity muscles that exhibit periods of negativity. For gravity force to assist the arm motion, the antigravity muscle activity should drop below the tonic level that would be required to compensate it and keep that arm motionless on a given posture. Such a neural

strategy is not suitable for the horizontal plane because muscles work perpendicular to gravity. Figure 3 (C and D) depicts the predictions of the Smooth-Effort model in all directions. These simulations reveal that among 16 possibilities, 2 movement phases (acceleration and deceleration) × 2 types of muscles × 4 movement directions, the model predicts two specific negative periods for antigravity muscles: during the acceleration of downward movements and during the deceleration of upward movements (purples areas in Fig. 3, C and D). Instead, the compensation hypothesis predicts phasic components of antigravity muscles that are always positive or equal to zero, i.e., no phasic component ever exhibits periods of negativity (see fig. S2, C and D).

In accord with the effort-optimization hypothesis, negative periods were frequent for antigravity muscles (Fig. 4, A and B; purple areas). The negativity of antigravity muscles precisely occurred when gravity effects could assist motion, that is, during the acceleration of downward movements (Fig. 4A) and the deceleration of upward movements (Fig. 4B). During those periods, the arm presumably falls free. Gravity muscles, whose effects can only add up to those of gravity, did not exhibit such negative periods (Fig. 4, C and D). Nor did any muscles for Earth-horizontal movements during which the task requires to compensate for gravity effects (Fig. 5). These qualitative results indicate that the presence of negative phasic EMG is specific to the earth-vertical plane and, even more specific, to the timing when gravity can assist movement, as predicted by the Smooth-Effort model. Further, it is independent of body orientation, and both species share it.

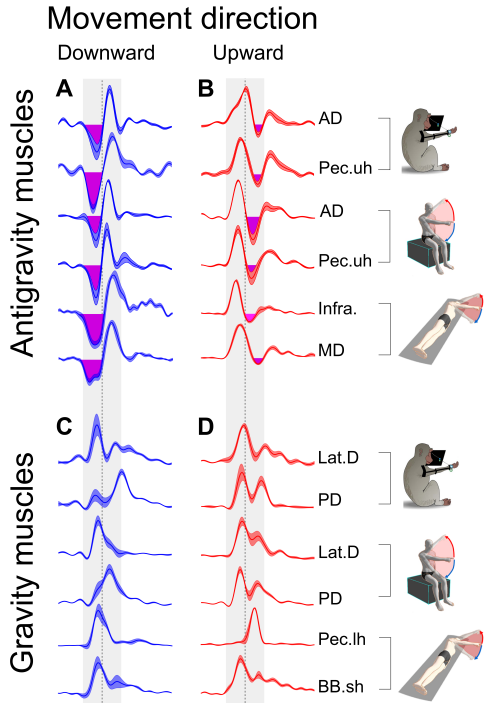

Fig. 4. Phasic EMG patterns of earth-vertical movements reveal gravitational force contribution to the motion of the arm. Mean (±SE) phasic EMGs recorded in monkeys ($n = 3$) and both groups of humans ($n = 8$ in each group) during earth-vertical movements. Left column (**A** and **C**) (blue traces) presents EMGs recorded during downward movements, while right column (**B** and **D**) (red traces) presents EMGs recorded during upward movements. Top row (A and B) presents EMG activations of antigravity muscles (pulling upward, against gravity): anterior deltoid (AD), upper head of Pectoralis major (Pec. uh), infraspinatus (Infra.), middle deltoid (MD). Those muscles pull against gravity, i.e., away from the final target during a downward movement and toward the final target during an upward movement. Bottom row (C and D) presents EMG activations of gravity muscles (pulling downward, with gravity): Latissimus dorsi (Lat.D), posterior deltoid (PD), lower head of Pectoralis major (Pec.lh), the short head of biceps brachii (BB.sh). Those muscles pull with gravity, i.e., toward the final target during a downward movement and away from the final target during an upward movement. Purple areas denote phases where epochs of negativity were detected (see Methods). Such epochs were precisely observed for antigravity muscles (A and B) during the acceleration of a downward movement and during the deceleration of an upward movement, i.e., when gravity effects can help the muscle and therefore discount muscle effort. EMG traces were aligned on movement onset and normalized in duration and amplitude before averaging between participants. The gray vertical areas denote movement duration (shifted 100-ms backward to account for the electromechanical delay), and the vertical dashed lines denote 50% of movement duration. Typical movement durations for monkeys and humans are detailed in table S1.

Quantification of occurrence, amplitude, and duration of negativity

The vast majority of movements performed in the earth-vertical plane exhibited this general muscular pattern. On average (±SD), across monkeys and humans, the phasic EMG of antigravity muscles exhibited negative values in 90.8 ± 2.7% and 72.1 ± 5.5% of downward and upward movements, respectively (see Fig. 6A and table S3 for all values). In contrast, in the earth-horizontal plane, rightward and leftward movements exhibited negative periods only in 0.014 ± 0.036% and 0.021 ± 0.048%, respectively (table S3).

An amplitude index quantified how much gravity force assisted muscle force. This index expressed antigravity muscles' activation levels relative to the theoretically required level for exact compensation of gravity effects (the tonic level; see Methods). An index value of −100% means utterly relaxed muscles; thus, the gravity force fully participated in arm movement. A value of 0% means that antigravity muscles are precisely compensated for gravity effects; thus, the gravity force did not produce any movement, as predicted by the compensation hypothesis. On average, across monkeys and humans, the amplitude index averaged (±SD) −90.7 ± 2.8% and −66.7 ± 9.6% for downward and upward movements, respectively (see Fig. 6B and table S3 for all values).

We also computed the duration of negative epochs and expressed it as a percentage of acceleration duration for downward movements and a percentage of deceleration duration for upward movements. On average (±SD), negative periods represented 60.7 ± 11.5% of downward acceleration duration and 43.1 ± 12.4% of upward deceleration duration (see Fig. 6C and table S3 for all values).

In both species, the occurrence and extent of negative periods reveal that the brain did not compensate for gravity force. Instead, it lets gravity force assisting muscle force. Next, we further demonstrate this by characterizing the temporal organization of agonist/antagonist muscular activation, which is the most basic and widely used descriptor of muscle patterns (*38*, *39*).

Gravity effects on muscular activation timing

Figure 7 summarizes the activation timings of agonist and antagonist muscles. "Agonist" and "antagonist" are generic denominations that respectively designate the muscles that pull toward or away from the final target. We found that this timing radically changes with movement direction (see tables S4 and S5 for all values and statistical comparisons). Most notably, it is the negativity of antagonist

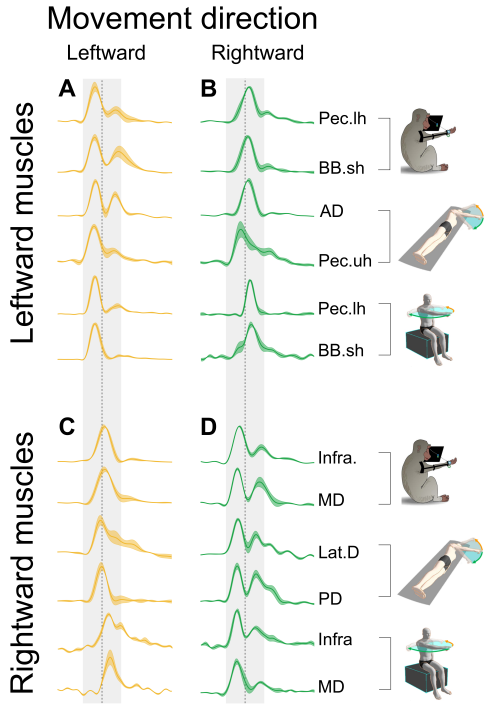

Fig. 5. Phasic EMG patterns of earth-horizontal movements. Same layout as Fig. 4. Mean (±SE) phasic EMGs are presented for monkeys ($n = 3$) and both groups of humans ($n = 8$ in each group). Left column (**A** and **C**) (yellow traces) presents EMGs recorded during leftward movements, and right column (**B** and **D**) (green traces) presents EMGs recorded during rightward movements. Top row (A and B) presents EMG activations of muscles pulling leftward. Those muscles pull perpendicularly to gravity, i.e., away from the final target during a rightward movement and toward the final target during a leftward movement. Bottom row (C and D) presents EMG activations of muscles pulling rightward. Those muscles also pull perpendicularly to gravity, i.e., toward the final target during a rightward movement and away from the final target during a leftward movement. No negative periods were detected during earth-horizontal movements, meaning that gravity effects (perpendicular to movement direction) were correctly compensated. EMG traces were aligned on movement onset and normalized in duration and amplitude before averaging between participants. The gray areas denote movement duration (shifted 50-ms backward to account for the electromechanical delay), and the earth-vertical dashed lines denote 50% of movement duration. Typical movement durations for monkeys and humans are detailed in table S1.

muscles (antigravity muscles, gray open circles) that governed the acceleration of downward movements (Fig. 7, blue arrow). During downward movements, both humans and monkeys activated their agonist muscles (gravity muscles, black filled squares) nearly at the time of movement initiation. Given electromechanical delays (*40*), this agonist activation occurs too late to participate in movement initiation. The delayed activation of gravity muscles (agonist) presumably complements the negativity of antigravity muscles (antagonist) to reach the appropriate movement speed (*41*, *42*). The organization of downward movements is in sharp contrast to earth-horizontal movements, where agonist activation generated acceleration force roughly 100 ms before movement onset (Fig. 7, yellow and green arrows).

Upward movements (red arrow) exhibited an organization that was the inverse of downward movements. First, the activation of agonist (antigravity) muscles occurred at a similar timing as earth-horizontal movements (black filled squares). Then, the agonist (antigravity) muscle became negative (gray open square). This late negativity lets gravity assist muscle force in decelerating the arm upward. Again, this is in sharp contrast to earth-horizontal movements, where the single activation of antagonist muscles produces the deceleration force.

Purple open symbols in Fig. 7 demonstrate that the Smooth-Effort model predicts deactivation timings that well match experimental data. According to the effort-optimization hypothesis, these negative periods reveal that the brain uses gravity to discount muscle force that pulls downward. Next, we directly test this hypothesis by within-muscle comparisons of EMG activities between earth-horizontal and earth-vertical movements.

Within-muscle comparisons between earth-horizontal and earth-vertical movements

Humans performed arm movements that were either parallel or perpendicular to the head/feet body axis, from two body orientations (Fig. 8, A and B). Because the same muscles were responsible for earth-vertical and earth-horizontal movements, one can directly compare the amplitude of muscular activations between movement planes. Specifically, we compared the activation of gravity muscles in the vertical plane to activation of the same muscles in reciprocal earth-horizontal movements (here, reciprocal refers to movements with the same direction in the ego-centered frame of reference). For example, in the ego-parallel group (Fig. 8A), one can compare the activation of agonist muscles between acceleration phases toward the feet in the two planes (blue versus green targets). If gravity effectively assists muscle force, one would expect reduced activation of gravity muscles in the earth-vertical plane compared to reciprocal movement in the earth-horizontal plane. Following this logic, data falling below the identity line indicate that earth-vertical movements necessitate weaker muscular activation than earth-horizontal ones. The Smooth-Effort model predicts such comparisons to fall below the identity line (see large purple diamonds in Fig. 8, C to F), as earth-vertical movements necessitate weaker muscular activations than earth-horizontal ones.

Figure 8 (C and D) compares downward movement acceleration to reciprocal movement acceleration in the earth-horizontal plane, for the ego-parallel group (Fig. 8A) and the ego-perpendicular group (Fig. 8B). All individual comparisons fall below the identity line ($n = 48$). This result demonstrates that downward acceleration required reduced agonist muscle activation compared to horizontal acceleration (all agonist muscles averaged per participant, Student paired two-sided; ego-parallel group, $T_7 = 6.4$, $P = 0.0004$; ego-perpendicular group, $T_7 = 9.6$, $P = 0.00003$; see bar graph insets in Fig. 8, C and D). Thus, gravity effectively assisted muscle force in accelerating the arm downward.

Figure 8 (E and F) compares the decelerations of upward movements and reciprocal movements in the earth-horizontal plane for the two groups. Forty-one of 48 individual comparisons fall below the identity line. The deceleration of upward movements required significantly reduced antagonist muscle activation compared to reciprocal horizontal deceleration (all antagonist muscles averaged, Student paired two-sided; ego-parallel group, $T_7 = 3.3$, $P = 0.01$; ego-perpendicular group, $T_7 = 8.0$, $P = 0.00009$; see bar graph insets in Fig. 8, E and F). Thus, gravity effectively assisted muscle force in decelerating the arm upward.

As predicted by the effort-optimization hypothesis, these results confirm that deactivating antigravity muscles (as revealed by phasic

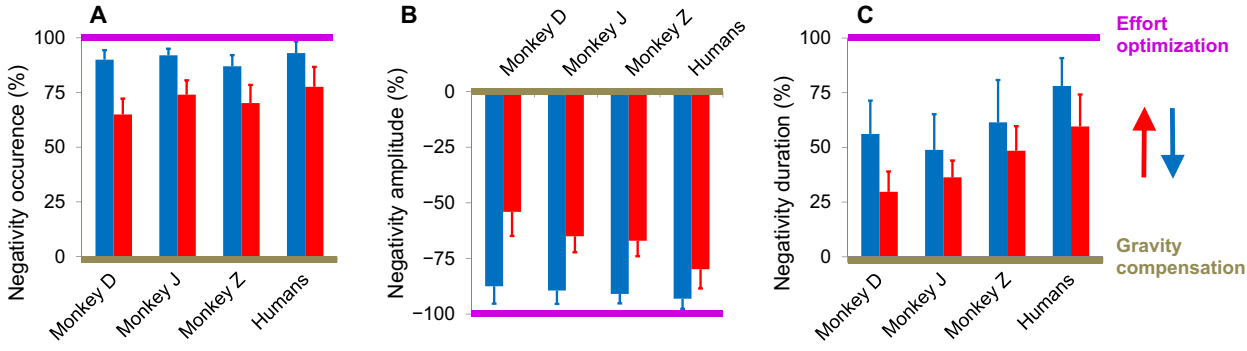

Fig. 6. Substantial negativity of phasic EMGs. Characterization of negative epochs recorded for antigravity muscles (the muscles pulling against gravity, presented in Fig. 4, A and B) during earth-vertical movements. Mean values (±SD) are presented for each monkey and all humans ($n = 16$). Colored arrows indicate movement directions (blue for downward; red for upward). (**A**) Mean occurrence percentage (number of positive detection/number of trial) of a negative phase for each monkey and humans. (**B**) Maximal negativity amplitude was expressed as a percentage of the subtracted tonic value (see Methods). A value of −100% means that the muscle was utterly relaxed. Thus, gravity maximally helped to move the arm. On the contrary, a value of 0% means that gravity effects were correctly compensated for by muscle force, as predicted by the compensation hypothesis. (**C**) Mean negative phase duration expressed as a percentage of the acceleration duration for downward movement and as a percentage of the deceleration duration for downward movements. Error bars represent the SD of the mean between recording sessions for each monkey and between participants for humans.

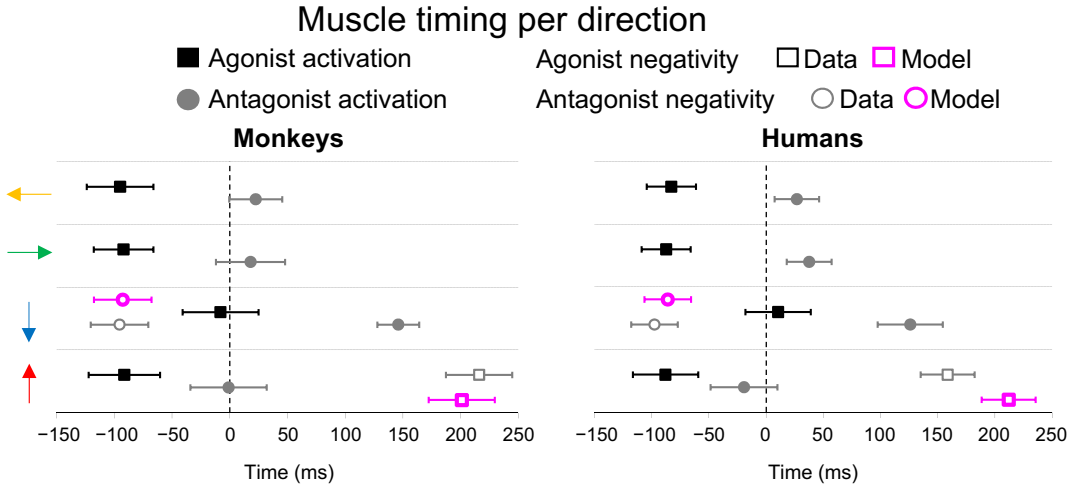

Fig. 7. Gravity shapes the temporal organization of muscular activation patterns. Mean (±SD) onset timings (see Methods) of agonist and antagonist muscles activations and negativity for monkeys (left, $n = 3$) and humans (right, $n = 16$). Negative phases being a discriminant prediction between the Effort-optimization model and the compensation model, their predicted timings are also depicted (purple symbols). Agonist and antagonist are generic denominations that respectively designate the muscles that pull toward or away from the final target. Muscular activity recorded in each movement direction is presented in separate rows (colored arrows indicate movement direction). EMG traces were aligned on movement onset. Antigravity muscle negativity timings closely match between experimental data and theoretical predictions.

EMG negativity) effectively reduces the muscular effort that pulls downward in gravity (not body) coordinates. The neural integration of gravity yields optimal motor planning.

DISCUSSION

Here, we investigated a fundamental question: Does the motor system compensate for the gravity force, or does it exploit it as a "free" force to discount muscle effort during movement? A combination of modeling, kinematics, and EMG analyses provided strong support for the Effort-optimization strategy. We analyzed multiple variables, but two stand out as most relevant: (i) the relative time to peak velocity unmasked the motor plan at the kinematic level; (ii) the negativity of the phasic EMG component revealed the neural signature of the optimal motor plan, where gravity is purposefully exploited for effort-efficient motor control.

As previously demonstrated, shorter acceleration duration and higher peak acceleration for upward than for downward movements is the kinematic signature of optimal integration of gravity into the motor plan [(*23*, *24*), see Fig. 3 and (*25*)]. If the motor system compensated for the gravity force, kinematics should be direction independent in the earth-vertical plane, as is the case in the earth-horizontal plane [see fig. S2 and (*20*, *21*)].

We sought the neural signature of this optimal motor plan by analyzing EMG activity patterns during single-degree-of-freedom movements to systematically vary the effect of gravity while the rest

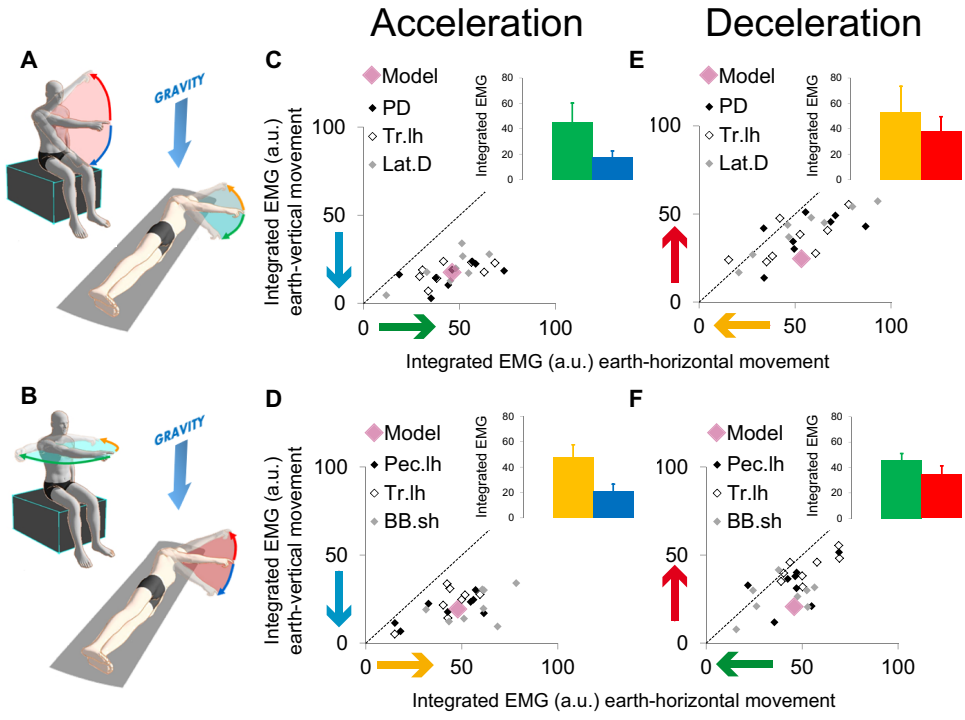

Fig. 8. Saving effects on muscles pulling downward. Activations of gravity muscles for both groups of humans during earth-vertical versus earth-horizontal movements. Experimental setup in the ego-parallel group (**A**) and in the ego-perpendicular group (**B**). Colored arrows indicate movement and gravity directions. (**C**) Ego-parallel group. For each participant ($n = 8$) and three gravity muscles (PD, posterior deltoid; Tr.lh, triceps long head; Lat.D, latissimus dorsi), normalized muscular activations integrated over the acceleration phase toward the feet are compared between body orientations. The bar graph inset presents means (±SD) of all muscles and participants. (**D**) Ego-perpendicular group ($n = 8$). Same organization as (C) for movements toward the left side of the body (Pec.lh, pectoralis lower head; Tr.lh, triceps long head; BB.sh, short head of biceps brachii). (**E**) Ego-parallel group. Same organization and muscles as (C) during the deceleration phase of leftward movements. (**F**) Ego-perpendicular group. Same organization and muscles as (D) during the deceleration phase of rightward movements. In (D) to (F), data points falling below the identity line (black dashed) mean that muscles are less activated in the vertical than in the horizontal plane. Experimental data support the predictions of the effort-optimization hypothesis (see model predictions, purple diamonds). a.u., arbitrary units.

of the movement dynamics (inertial forces) remained constant. Our rationale was straightforward. If the brain truly exploits the gravity force to discount muscular effort, specific and time-locked negative periods should appear in the phasic EMG signal. As predicted by the Smooth-Effort model (Fig. 3), we found that antigravity muscles exhibited periods of negativity time-locked to the acceleration phase of a downward movement and the deceleration phase of an upward movement, precisely when gravity is predicted to assist the movement (Figs. 4 and 5). In particular, the model predicted two specific periods of negativity out of 16 possibilities: 4 directions (upward, downward, rightward, or leftward) × 2 types of muscles (gravity or antigravity muscles) × 2 movement phases (acceleration or deceleration). We demonstrated that the negativity of the phasic EMG component was both consistent and extensive (Fig. 6), significantly affected the temporal organization of the muscle patterns (Fig. 7), and decreased the activation of gravity muscles (the muscles pulling with gravity; Fig. 8). These results provide strong support for the active participation of gravity effects to movement generation. In both macaques and humans, direction-dependent kinematic and muscular patterns point toward a motor strategy that optimizes gravity effects to discount muscle effort.

Notably, many studies have previously observed negativity of the phasic component of muscular activation for vertical movements (*13*, *15*, *34*, *36*). However, this phenomenon was primarily ignored and attributed to erratic errors in the separation of noisy signals. The present study demonstrates that negativity is not erratic but systematic.

EMG to force interpretation pitfalls

An important pitfall when using EMG activity as a proxy for muscle force is that several extrinsic and intrinsic factors—e.g., the electrode impedance, its position with respect to the muscle, the type and angle of muscle fibers—influence the EMG to force relationship (*43*). In addition, force production depends on a muscle's length and velocity (*44*, *45*). Muscles produce greater forces at intermediate than shortest and longest lengths. Muscles also produce greater forces in eccentric contraction mode (when lengthening, i.e., negative velocity) than in isometric (zero velocity) or concentric contraction modes (when shortening, i.e., positive velocity). At the beginning of a downward movement, antigravity muscles work in eccentric mode (they are contracted while lengthening), but less so in the earth-horizontal plane where antigravity muscles are less contracted. In addition, the load force on antigravity muscles must slightly change muscle fascicle length in the earth-vertical, compared to the earth-horizontal, plane. To some extent, during the acceleration of a downward movement, the negativity of antigravity muscles could thus reflect that the muscle is moved to a more favorable part of its force-length and/or force-velocity relationship, allowing the muscle to compensate for gravity effects with less EMG activation.

However, the abovementioned confounding factors cannot explain several of the current findings. First, the comparison of gravity muscle activation (Fig. 8), showing that direction-dependent motor patterns effectively saved muscle efforts that pull downward, was made on muscles with identical contraction modes and lengths (no loading on these muscles). Second, the negativity of antigravity muscles preceded downward movement onset, at a time that force production mechanisms were unchanged. Third, the activation of gravity muscles during downward movements was delayed such that it could not produce the initial part of the motion. Fourth, the negativity of antigravity muscles during downward movements revealed a 90% drop in activity from the level needed to compensate for gravity torque. Compared to an isometric contraction, the eccentric contraction mode is known to increase muscle force by only 10%, at best (*46*, *47*). Even adding a slight muscle length increase due to preloading in the vertical plane would be far from explaining the huge muscle activation drop observed (*48*). Fifth, the negativity of antigravity muscles was observed during upward movements, when these muscles work in concentric mode. Thus, a more favorable force-velocity eccentric contraction is not necessary to produce the negativity of antigravity muscles.

Significance and limits of the optimality interpretation

It is important to emphasize that the present results deny the compensation hypothesis during the motion only. Compensating gravity effects remains necessary to keep the arm static during initial and final postures. Moving and holding still—on initial and final postures—is thought to rely on distinct processes (*49*–*51*).

Simulations from the Effort-optimization model did not have to assume any complex muscle dynamics. Instead, we modeled the muscle dynamics as a simple low-pass filter [see Methods and (*52*, *53*)]. This makes interpretations straightforward because the model predictions actually reflect pure physics. However, the simple muscle model used here has some limitations. The Effort-optimization model does not reproduce certain aspects of the experimentally recorded muscle patterns, e.g., it does not predict the coactivation of antagonistic muscles, as simultaneous activation of muscles pulling in opposed directions is inherently effortful and, thus, nonoptimal. However, this would affect all movement directions equally, whereas our arguments are based on comparisons between directions, where such nonspecific model limitations are unrelated to the hypotheses tested in this study.

To explain the rich motor adaptation capabilities exhibited by humans and other biological systems, some models have minimized composite costs functions, i.e., the blend of multiple subcosts such as effort, smoothness, end-point variance, or time (*54*, *55*). Coactivation of antagonistic muscles has long been suggested to protect joints against mechanical stress (*56*). It is also useful for minimizing end-point variance in a stochastic context accounting for sensorimotor noise and conduction delays (*57*, *58*). Future work shall integrate joint stress or end-point variance as cost functions to build models that more thoroughly explain biological motor patterns.

Given the richness of humans' and monkeys' motor repertoires, the study of monoarticular arm movements may seem restrictive. However, it is essential to point out that direction-dependent motor patterns have been observed for movements as varied as monoarticular upper limb (*21*, *23*, *59*), multiarticular upper limb (*60*, *61*), and whole-body movements (*62*). These direction-dependent motor patterns are optimal to save muscle effort and slowly reoptimize to newly experienced gravito-inertial fields (*23*, *24*, *60*). Thus, the present results, along with previous ones, provide conceptual support for a general theory that the brain builds internal representations of the environmental and musculoskeletal dynamics to optimize motor planning and control (*1*, *2*, *27*, *63*).

Between-species comparisons

Although humans and monkeys are close relatives, significant structural differences exist between their brains (*64*, *65*). The present results reveal that monkeys produce the same direction-dependent kinematics as humans (Fig. 2), revealing that optimal motor planning in the gravity field is a shared process between primate species. In both species, motor patterns well matched the prediction of the effort-optimization hypothesis. Comparing the directional effect between humans and monkeys did not reveal any significant difference (table S6).

It would be interesting to also study gravity-related motor control in nonprimate species, as the neural control of movements may differ in small and larger animals because of the difference in the relative importance of passive joint internal (e.g., stiffness) versus external forces (*66*–*68*). Although macaques are 10 times lighter than humans, they still take advantage of gravity effects to minimize muscle effort. Testing the effects of increased load forces on body limbs of smaller animals may offer exciting insights into the neural underpinning of motor reoptimization (*69*).

Optimal control is thought to represent the finest stage of motor learning. This stage is supposedly only attainable after sufficient practice has been achieved to attain the task goal at a greater expense (*70*, *71*). This view can be formalized as a dual process where one pathway first learns an accurate forward model and the second pathway then derives an optimal motor plan (*27*). Although the neurophysiological bases of the first pathway (forward model) have been extensively studied, the neurophysiology of the second one is essentially unknown. The demonstration that macaque arm movements share the same properties as humans opens a door for new studies in monkeys that could probe the neural underpinnings of optimal motor control. Several studies have provided neurophysiological evidence of gravity internalization in macaques and humans (*5*–*9*, *72*, *73*). The fact that both macaques and humans share this strategy underlines the fundamental influence of gravity on the evolution, development, and function of motor systems. Because the metabolic rate influences body size, resource use, rate of senescence, and survival probability (*74*–*79*), preserving muscle effort may represent an essential pursuit for the brain (*28*, *80*–*85*).

METHODS

Monkeys and humans performed standard experiments as previously described elsewhere [for humans, see (*20*, *22*); for monkeys, see (*86*, *87*)].

Monkey experiments

Setup

Three rhesus monkeys (Macaca Mullata; 5.5 to 7.2 kg) participated in the study after the approval of all the experimental procedures by the Animal Studies Committee and Institutional Animal Care and Use Committee. Monkeys were head-fixed and seated in a custom-made primate chair anchored to a virtual reality system. A mirror mounted in front of the monkey's face at an angle of 45°, reflected

the display of a monitor. Monkeys wore custom-made glasses (Kodak Wratten filters red #29 and green #61), such that visual stimulus rendered in three dimensions as red-green anaglyphs. Using an optoelectronic tracking system (NDI Optotrak Certus), the three-dimensional (3D) position of the monkey's right hand was fed back in real time on the monitor as a cursor sphere (1-cm radius). The monkey performed the task using his right arm. A custom-made brace was positioned on the monkey's right arm to restrain the elbow and wrist joints, allowing motion of the arm around the shoulder joint only (Fig. 1A).

Task

By operant conditioning, we trained three monkeys to perform fast point-to-point single degree of freedom reaching movements (shoulder rotations) between sets of two targets (1-cm radius), from an initial to a final target. We positioned the targets at arm's length. For upward and downward movements (earth-vertical plane), we set up two targets in a parasagittal plane crossing the center of rotation of the animal's right shoulder joint. We horizontally aligned the upper target with the animal's shoulder (arm horizontal: 90° shoulder elevation, 0° shoulder abduction). We positioned the lower target such that the shoulder was extended by 20° below horizontal (70° shoulder elevation, 0° shoulder abduction). Accordingly, an upward movement consisted of a 20° shoulder flexion and a downward movement consisted of a 20° shoulder extension (elbow being fully extended and midpronated). For rightward and leftward movements, we set up three targets in a transverse plane crossing the center of rotation of the animal's shoulders. The central-starting target was the same as the upper target for earth-vertical movements (90° shoulder elevation, 0° shoulder abduction). We also set up two additional targets at an angle of 20° rightward (90° shoulder elevation, 20° shoulder abduction) and 20° leftward (90° shoulder elevation, 20° shoulder adduction), taking as reference the horizontal position of the arm on the central target. A rightward movement consisted of a 20° abduction (starting at the central and ending at the most rightward target), and a leftward movement consisted of a 20° adduction (starting at the central and ending at the most leftward target). Monkeys performed 200 to 300 trials per session (total number of trials recorded for each monkey: $D = 2854$; $J = 2347$; $Z = 2987$).

Kinematic recording

We used an optoelectronic tracking system (NDI Optotrak Certus, 200 Hz) to record the 3D position of infrared emitting diodes (markers) taped on the animal arm and brace. The most distal marker was used to provide the hand position feedback to the monkey.

Electromyographic recording

We recorded EMG activity with pairs of insulated single-stranded stainless steel wires (A-M SYSTEMS, 790700). Before the experiment, we inserted two twisted wires (3-mm uninsulated at their ends) in each targeted muscle (1-cm separation) using 33G hypodermic needles [TSK STERiJECT; for further details, see (*86*)]. We plugged the wires into a custom-made printed circuit board, itself linked to a differential EMG amplifier (GRASS TECHNOLOGIES, QP511). Then, to verify the appropriate positioning of each electrode, we induced muscle twitch using microstimulations. The Optotrak (ODAU, NDI) sampled the raw EMG activity at 4 kHz, synchronously with kinematic signals. We recorded activation patterns of the following 11 muscles: deltoids (anterior, middle, and posterior), triceps (long and lateral heads), biceps (two heads), pectoralis major (upper and lower), latissimus dorsi, and infraspinatus.

Human experiments

Sixteen participants (four females; mean age, 25.4 ± 5.5 years; mean weight, 74.2 ± 9.6 kg; mean height, 168 ± 32 cm) voluntarily participated in the experiments. All participants were right-handed (*88*) with normal or corrected to normal vision and did not have any neurological or muscular disorders. The local ethics committee approved the experimental protocol that was carried out in agreement with legal requirements and international norms (Declaration of Helsinki, 1964).

Experimental protocol

Participants performed single-degree-of-freedom arm movements with their elbow fully extended and midpronated (shoulder rotations). We randomly separated the 16 participants into two groups of eight each. Participants from the "ego-parallel" group performed arm movements in the parasagittal plane crossing their right shoulder (Fig. 1B). Participants from the "ego-perpendicular" group performed arm movements in the transversal plane crossing their right shoulder (Fig. 1C). For each participant, we positioned three targets in the movement plane corresponding to the respective group. For both groups, the central target implied a 90° shoulder elevation and a 0° shoulder abduction (arm perpendicular to the trunk; dark arm in Fig. 1, B and C). From this central target, the other two targets triggered 20° shoulder rotations that were opposite in the plane of motion (light arms in Fig. 1, B and C).

Participants performed arm pointing movements in two conditions of body orientation (Fig. 1, B and C). In one condition, they sat upright with their head-feet body axis parallel to gravity. In the other condition, they were 90° rotated in roll and lied on their left side with the head-feet body axis perpendicular to gravity. Between body orientation conditions, target position was kept constant in the participant egocentric frame of reference (targets rotated with the participant). Half of the experiment consisted of arm movements that were parallel to the gravity vector (seating upright in the ego-parallel group and lying on the side in the ego-perpendicular group). The other half consisted of arm movements that were perpendicular to it (lying on the side in the ego-parallel group and seating upright in the ego-perpendicular group). We counterbalanced the order of body orientation conditions between participants.

We instructed participants to perform accurate and uncorrected arm movements at fast speed. Before the experiment, participants performed as much practice trials as they wanted to familiarize with the task. Then, for each body orientation, participants performed 60 trials (30 in each direction) in a randomized order (30 trials × 2 body orientations × 2 directions × 16 participants = 1920 trials). Each trial took place as follows. The participant pointed at the central target and held it. After a random delay time (1 to 2 s), he/she received instructions about which target to point. The participant performed the movement and held the final position until the experimenter stopped the recording and informed him/her to relax.

Kinematic recording

We used an optoelectronic tracking system (eight cameras, 200 Hz; Vicon, Oxford, UK) to record the position five reflective markers taped on the participants' arm: shoulder (acromion), elbow (lateral epicondyle), wrist (between the cubitus and radius styloid processes), hand (first metacarpophalangeal joint), and the nail of the index fingertip.

Electromyographic recording

We used bipolar surface electrodes (IT, 2000 Hz; Aurion, ZeroWire EMG) to record EMG activity. The GIGANET unit (Vicon, Oxford, UK) allowed synchronously recording EMG and kinematic data. We

placed the electrodes on the following 12 muscles: deltoids (anterior, middle, and posterior), triceps (long and lateral heads), biceps (two heads), brachioradialis, infraspinatus, pectoralis major (upper and lower heads), and latissimus dorsi.

Data analysis

We processed kinematic and EMG data using custom MATLAB scripts (MathWorks). As monkey and human data were processed similarly, we describe the data analysis for both experiments in a single section.

Kinematics

Kinematic data processing was similar to previous studies (*22*, *23*). We filtered the position (low-pass, 5-Hz cutoff, fifth-order, zero-phase distortion, "butter" and "filtfilt" functions) before differentiation. A 10% threshold of the peak angular velocity defined movement onset and offset. We rejected from further analyses trials where the velocity profile presented more than one local maxima (on average, <5% of trials in monkeys and <2% of trials in humans). We then calculated the following parameters (fig. S1): movement duration, movement amplitude, peak acceleration, and relative duration to peak acceleration (rDPA, duration to peak acceleration/movement duration), peak velocity and relative duration to peak velocity (rDPV, duration to peak velocity/movement duration). We also computed angular joint displacements to control that shoulder internal/external rotations, as well as wrist or elbow rotations, were negligible.

Electromyograms

We first rectified and filtered EMG signals (bandpass 20 to 300 Hz, third-order, zero-phase distortion, "butter" and "filtfilt" functions). Then, we integrated this signal over 5-ms bins and cut it off 500 ms before movement onset and 500 ms after movement offset. To compare EMGs between muscles, participants, and datasets, we normalized each trace by the maximum value observed for the corresponding muscle in the dataset. We then averaged trials across three repetitions, resulting in 10 averaged trials to be analyzed.

We used a well-known subtraction procedure that was proposed to isolate the phasic and tonic components of the full EMG signal (*13*, *15*, *34*, *36*, *37*). We computed the average values of the integrated EMG signals from 1 to 0.5 s before movement onset and from 0.5 to 1 s after movement offset (fig. S3). We used these average values to compute the tonic component as a linear interpolation between them. Last, we computed the phasic component by subtracting the tonic component from the full integrated EMG signal.

We quantified the negativity of the phasic muscular activations by calculating the following parameters: (i) the duration of the negative epoch, defined as the time interval where the phasic activity dropped below zero minus the 95% confidence interval (computed on the integrated EMG signals from 1 to 0.5 s before movement onset) and this for longer than 40 ms; (ii) an index of the amplitude of the negative epoch, computed as follows

$$\mathrm{PminT} \times 100$$

where Pmin is the phasic maximally negative value (during the negative epoch), and T is the tonic value subtracted at the time of Pmin. An amplitude index value of −100% means that muscles were completely relaxed and that the gravity force fully participated in generating the arm motion. A value of 0% means that antigravity muscles precisely compensated for gravity force, i.e., that gravity did not produce any arm motion; (iii) the frequency with which a negative phase was detected among all trials.

We also characterized muscular activation using the following parameters: (iv) the onset of muscle activation, defined as the time where the phasic activity first rose above zero plus the 95% confidence interval (computed on the integrated EMG signals from 1 to 0.5 s before movement onset) for longer than 40 ms; (v) the mean normalized integrated signal over the acceleration period (from movement onset minus 100 ms to time to peak velocity minus 100 ms); (vi) the mean normalized integrated signal over the deceleration period (from the time to peak velocity minus 100 ms to movement offset minus 100 ms).

Statistics

We checked that all variables were normally distributed (Shapiro-Wilk *W* test) and that their variance was equivalent (Mauchly's test). We used repeated measure analysis of variance (ANOVA), applied to means of separate sessions in each monkey, as well as mean values for each human subject. Post hoc comparisons were performed using Scheffé tests. Student paired two-sided tests were used to compare muscle activation levels between body orientations in humans. In all cases, the level of significance was equal to 0.05. To compare results between species, we used Mann-Whitney *U* test, and we corrected comparisons for multiple tests using Bonferroni correction.

Simulations

We used the optimal control framework to compare the Effort-optimization and Compensation hypotheses by predicting movement kinematics and muscle patterns. The effort-optimization hypothesis is simulated on the basis of muscle effort minimization: the Smooth-Effort model (*23*, *24*). More advanced versions of this model have been shown to account for multidegree of freedom arm movements (*25*, *53*). The compensation hypothesis is simulated on the basis of a model that leads to compensation of gravitational torques, the Minimum Jerk (*33*), which minimizes a single kinematic cost related to smoothness. Therefore, it does not seek to exploit gravity effects in the movement plan. We used the same models as in Gaveau *et al.* (*24*) but extended our analysis to muscle patterns. The musculoskeletal dynamics of the arm was modeled as follows

$$\tau_{ag} - \tau_{ant} = I\ddot{\theta} + B\dot{\theta} + \mathrm{GT}(\theta) \quad (1)$$

$$\tau_{ag} - \tau_{ant} = \rho(a_{ag} - a_{ant}) \quad (2)$$

$$\sigma \dot{a}_{ag} = u_{ag} - a_{ag} \quad (3)$$

$$\sigma \dot{a}_{ant} = u_{ant} - a_{ant} \quad (4)$$

where τ_{ag} is the agonist torque, τ_{ant} is the antagonist torque, θ is the joint angle with respect to the horizontal, I is the moment of inertia with respect to the (fixed) center of rotation, $B = 0.87\ \mathrm{kg \cdot m^2/s}$ is the viscous friction coefficient (*89*), $\mathrm{GT}(\theta)$ is the gravitational torque, $\rho = 100\ \mathrm{N \cdot m}$ is a gain factor, a_{ag} is the agonist muscle activation, a_{ant} is the antagonist muscle activation, and $\sigma = 0.04$ s is the time constant of the muscle dynamics.

Equation 1 describes the equation of motion for a single degree of freedom rigid body movement. The expression of the gravitational torque is given by $\mathrm{GT}(\theta) = mgl_c \cos\theta$ where m, g, and l_c are respectively the mass, gravity acceleration, and length to the center of mass of the arm. In Eq. 2, the constant ρ is a gain factor relating agonist

and antagonist muscle activations to joint torques. Equations 3 and 4 describe the muscle dynamics. The control variable is $\boldsymbol{u} = (u_{ag}, u_{ant})^T$, the muscles being modeled as first-order low-pass filters. It can be thought as the inputs to the motor neurons for which we imposed the constraint $(u_{ag}, u_{ant}) \in [0,1]^2$. This implies the non-negativity of each muscle activation and, therefore, of each muscle torque. The net torque is simply obtained by subtracting the agonist and antagonist torques (i.e., $\tau_{ag} - \tau_{ant}$).

To formulate optimal control problem and test our hypothesis, it is also necessary to define cost functions. Here, the Smooth-Effort model minimizes a composite cost combining effort and smoothness. The muscle effort associated to a movement is computed as the absolute work of the agonist and antagonist muscle torques as follows

$$C_{\text{effort}} = \int_0^T |\tau_{ag}\dot{\theta}| + |\tau_{ant}\dot{\theta}|\, dt \quad (5)$$

Previous studies have shown that considering effort expenditure alone usually fails to account for motion smoothness (*90*). Accordingly, we considered that a complementary objective of motor planning seeks to maximize motion smoothness. This was achieved by penalizing large angle jerks. Thus, the additional term entering into the cost function is

$$C_{\text{smooth}} = \int_0^T (d\ddot{\theta}/dt)^2\, dt \quad (6)$$

The Smooth-Effort model then relies on the following composite cost function

$$C = C_{\text{effort}} + \alpha\, C_{\text{smooth}} \quad (7)$$

where α weights the relative magnitude of each subcost in the total cost function. On the basis of results from previous work (*30*) and to reproduce the present kinematic asymmetries, for all simulations, we set $\alpha = 8 \times 10^{-5}$. Previous modeling work on muscle activations has shown that muscle inactivation is the signature of an effort-like cost minimization (*25*). Previous modeling work on arm kinematics has also demonstrated that direction-dependent motor patterns do not emerge from the smooth part of the hybrid cost but from the effort part (*24*). Increasing alpha—i.e., the weight of the smooth cost—progressively decreased directional asymmetries. In the present study, we verified that this effect extended to muscle patterns. Increasing alpha progressively decreased the negativity of the antigravity muscle and progressively increased the activation of the gravity muscle. In fig. S2, we also present the results of the Minimum Jerk model alone (smooth cost alone, C_{smooth}) to simulate the compensation hypothesis (*33*).

SUPPLEMENTARY MATERIALS

Supplementary material for this article is available at http://advances.sciencemag.org/cgi/content/full/7/15/eabf7800/DC1

View/request a protocol for this paper from *Bio-protocol*.

REFERENCES AND NOTES

1. D. W. Franklin, D. M. Wolpert, Computational mechanisms of sensorimotor control. *Neuron* **72**, 425–442 (2011).
2. R. Shadmehr, M. A. Smith, J. W. Krakauer, Error correction, sensory prediction, and adaptation in motor control. *Annu. Rev. Neurosci.* **33**, 89–108 (2010).
3. O. White, J. Gaveau, L. Bringoux, F. Crevecoeur, The gravitational imprint on sensorimotor planning and control. *J. Neurophysiol.* **124**, 4–19 (2020).
4. J. R. Lackner, P. A. DiZio, Aspects of body self-calibration. *Trends Cogn. Sci.* **4**, 279–288 (2000).
5. D. E. Angelaki, A. G. Shaikh, A. M. Green, J. D. Dickman, Neurons compute internal models of the physical laws of motion. *Nature* **430**, 560–564 (2004).
6. J. Laurens, B. Kim, J. D. Dickman, D. E. Angelaki, Gravity orientation tuning in macaque anterior thalamus. *Nat. Neurosci.* **19**, 1566–1568 (2016).
7. J. Laurens, H. Meng, D. E. Angelaki, Neural representation of orientation relative to gravity in the macaque cerebellum. *Neuron* **80**, 1508–1518 (2013).
8. I. Indovina, V. Maffei, G. Bosco, M. Zago, E. Macaluso, F. Lacquaniti, Representation of visual gravitational motion in the human vestibular cortex. *Science* **308**, 416–419 (2005).
9. W. L. Miller, V. Maffei, G. Bosco, M. Iosa, M. Zago, E. Macaluso, F. Lacquaniti, Vestibular nuclei and cerebellum put visual gravitational motion in context. *J. Neurophysiol.* **99**, 1969–1982 (2008).
10. C. Rousseau, L. Fautrelle, C. Papaxanthis, L. Fadiga, T. Pozzo, O. White, Direction-dependent activation of the insular cortex during vertical and horizontal hand movements. *Neuroscience* **325**, 10–19 (2016).
11. C. G. Atkeson, J. M. Hollerbach, Kinematic features of unrestrained vertical arm movements. *J. Neurosci.* **5**, 2318–2330 (1985).
12. M. J. Hollerbach, T. Flash, Dynamic interactions between limb segments during planar arm movement. *Biol. Cybern.* **44**, 67–77 (1982).
13. M. Flanders, U. Herrmann, Two components of muscle activation: Scaling with the speed of arm movement. *J. Neurophysiol.* **67**, 931–943 (1992).
14. N. Kadmon Harpaz, T. Flash, I. Dinstein, Scale-invariant movement encoding in the human motor system. *Neuron* **81**, 452–462 (2014).
15. E. V. Olesh, B. S. Pollard, V. Gritsenko, Gravitational and dynamic components of muscle torque underlie tonic and phasic muscle activity during goal-directed reaching. *Front. Hum. Neurosci.* **11**, 474 (2017).
16. J. L. Cook, S. J. Blakemore, C. Press, Atypical basic movement kinematics in autism spectrum conditions. *Brain* **136**, 2816–2824 (2013).
17. R. Edey, J. Cook, R. Brewer, G. Bird, C. Press, Adults with autism spectrum disorder are sensitive to the kinematic features defining natural human motion. *Autism Res.* **12**, 284–294 (2019).
18. T. Krabben, G. B. Prange, B. I. Molier, A. H. Stienen, M. J. Jannink, J. H. Buurke, J. S. Rietman, Influence of gravity compensation training on synergistic movement patterns of the upper extremity after stroke, a pilot study. *J. Neuroeng. Rehabil.* **9**, 44 (2012).
19. S. Raj, N. Dounskaia, W. W. Clark, A. Sethi, Effect of stroke on joint control during reach-to-grasp: A preliminary study. *J. Mot. Behav.* **52**, 294–310 (2020).
20. R. Gentili, V. Cahouet, C. Papaxanthis, Motor planning of arm movements is direction-dependent in the gravity field. *Neuroscience* **145**, 20–32 (2007).
21. A. B. Le Seac'h, J. McIntyre, Multimodal reference frame for the planning of vertical arms movements. *Neurosci. Lett.* **423**, 211–215 (2007).
22. J. Gaveau, C. Papaxanthis, The temporal structure of vertical arm movements. *PLOS ONE* **6**, e22045 (2011).
23. J. Gaveau, B. Berret, L. Demougeot, L. Fadiga, T. Pozzo, C. Papaxanthis, Energy-related optimal control accounts for gravitational load: Comparing shoulder, elbow, and wrist rotations. *J. Neurophysiol.* **111**, 4–16 (2014).
24. J. Gaveau, B. Berret, D. E. Angelaki, C. Papaxanthis, Direction-dependent arm kinematics reveal optimal integration of gravity cues. *eLife* **5**, e16394 (2016).
25. B. Berret, C. Darlot, F. Jean, T. Pozzo, C. Papaxanthis, J. P. Gauthier, The inactivation principle: Mathematical solutions minimizing the absolute work and biological implications for the planning of arm movements. *PLOS Comput. Biol.* **4**, e1000194 (2008).
26. R. Shadmehr, F. A. Mussa-Ivaldi, Adaptive representation of dynamics during learning of a motor task. *J. Neurosci.* **14**, 3208–3224 (1994).
27. J. Izawa, T. Rane, O. Donchin, R. Shadmehr, Motor adaptation as a process of reoptimization. *J. Neurosci.* **28**, 2883–2891 (2008).
28. J. C. Selinger, S. M. O'Connor, J. D. Wong, J. M. Donelan, Humans can continuously optimize energetic cost during walking. *Curr. Biol.* **25**, 2452–2456 (2015).
29. N. Bernstein, *The Coordination and Regulation of Movements* (Oxford, 1967).
30. E. Burdet, R. Osu, D. W. Franklin, T. E. Milner, M. Kawato, The central nervous system stabilizes unstable dynamics by learning optimal impedance. *Nature* **414**, 446–449 (2001).
31. D. A. Hagen, F. J. Valero-Cuevas, Similar movements are associated with drastically different muscle contraction velocities. *J. Biomech.* **59**, 90–100 (2017).
32. J. A. Kelso, D. L. Southard, D. Goodman, On the nature of human interlimb coordination. *Science* **203**, 1029–1031 (1979).
33. T. Flash, N. Hogan, The coordination of arm movements: An experimentally confirmed mathematical model. *J. Neurosci.* **5**, 1688–1703 (1985).
34. C. A. Buneo, J. F. Soechting, M. Flanders, Muscle activation patterns for reaching: The representation of distance and time. *J. Neurophysiol.* **71**, 1546–1558 (1994).
35. M. Flanders, J. J. Pellegrini, J. F. Soechting, Spatial/temporal characteristics of a motor pattern for reaching. *J. Neurophysiol.* **71**, 811–813 (1994).

36. A. d'Avella, L. Fernandez, A. Portone, F. Lacquaniti, Modulation of phasic and tonic muscle synergies with reaching direction and speed. *J. Neurophysiol.* **100**, 1433–1454 (2008).
37. G. B. Prange, L. A. Kallenberg, M. J. Jannink, A. H. Stienen, H. van der Kooij, M. J. Ijzerman, H. J. Hermens, Influence of gravity compensation on muscle activity during reach and retrieval in healthy elderly. *J. Electromyogr. Kinesiol.* **19**, e40–e49 (2009).
38. A. Berardelli, M. Hallett, J. C. Rothwell, R. Agostino, M. Manfredi, P. D. Thompson, C. D. Marsden, Single-joint rapid arm movements in normal subjects and in patients with motor disorders. *Brain* **119**, 661–674 (1996).
39. E. Chiovetto, B. Berret, T. Pozzo, Tri-dimensional and triphasic muscle organization of whole-body pointing movements. *Neuroscience* **170**, 1223–1238 (2010).
40. P. R. Cavanagh, P. V. Komi, Electromechanical delay in human skeletal muscle under concentric and eccentric contractions. *Eur. J. Appl. Physiol. Occup. Physiol.* **42**, 159–163 (1979).
41. H. J. Hufschmidt, T. Hufschmidt, Antagonist inhibition as the earliest sign of a sensory-motor reaction. *Nature* **174**, 607 (1954).
42. R. Agostino, M. Hallett, J. N. Sanes, Antagonist muscle inhibition before rapid voluntary movements of the human wrist. *Electroencephalogr. Clin. Neurophysiol.* **85**, 190–196 (1992).
43. C. J. De Luca, The use of surface electromyography in biomechanics. *J. Appl. Biomech.* **13**, 135–163 (1997).
44. A. V. Hill, *First and Last Experiments in Muscle Mechanics* (Cambridge Univ. Press, UK, 1970).
45. A. M. Gordon, A. F. Huxley, F. J. Julian, The variation in isometric tension with sarcomere length in vertebrate muscle fibres. *J. Physiol.* **184**, 170–192 (1966).
46. S. Colson, M. Pousson, A. Martin, J. Van Hoecke, Isokinetic elbow flexion and coactivation following eccentric training. *J. Electromyogr. Kinesiol.* **9**, 13–20 (1999).
47. B. M. Papotto, T. Rice, T. Malone, T. Butterfield, T. L. Uhl, Reliability of isometric and eccentric isokinetic shoulder external rotation. *J. Sport Rehabil.* **25**, 2015-0046 (2016).
48. J. E. Langenderfer, C. Patthanacharoenphon, J. E. Carpenter, R. E. Hughes, Variability in isometric force and moment generating capacity of glenohumeral external rotator muscles. *Clin. Biomech.* **21**, 701–709 (2006).
49. R. Shadmehr, Distinct neural circuits for control of movement vs. Holding still. *J. Neurophysiol.* **117**, 1431–1460 (2017).
50. S. T. Albert, A. Hadjiosif, J. Jang, J. W. Krakauer, R. Shadmehr, Holding the arm still through subcortical mathematical integration of cortical commands. *bioRxiv* 10.1101/556282 , (2019).
51. T. Oya, T. Takei, K. Seki, Distinct sensorimotor feedback loops for dynamic and static control of primate precision grip. *Commun. Biol.* **3**, 156 (2020).
52. F. C. T. van der Helm, L. A. Rozendaal, *Biomechanics and Neural Control of Posture and Movement* (Springer-Verlag, New York, 2000).
53. J. Gaveau, C. Paizis, B. Berret, T. Pozzo, C. Papaxanthis, Sensorimotor adaptation of point-to-point arm movements after spaceflight: The role of internal representation of gravity force in trajectory planning. *J. Neurophysiol.* **106**, 620–629 (2011).
54. S. Gielen, Review of models for the generation of multi-joint movements in 3-D. *Adv. Exp. Med. Biol.* **629**, 523–550 (2009).
55. J. Gaveau, L. Demougeot, B. Berret, L. Fadiga, T. Pozzo, C. Papaxanthis, *21st NCM Annual Conference* (Society for the Neural Control of Movement, Puerto Rico, 2011).
56. C. Alessandro, B. A. Rellinger, F. O. Barroso, M. C. Tresch, Adaptation after vastus lateralis denervation in rats demonstrates neural regulation of joint stresses and strains. *eLife* **7**, e38215 (2018).
57. P. L. Gribble, L. I. Mullin, N. Cothros, A. Mattar, Role of cocontraction in arm movement accuracy. *J. Neurophysiol.* **89**, 2396–2405 (2003).
58. B. Berret, F. Jean, Stochastic optimal open-loop control as a theory of force and impedance planning via muscle co-contraction. *PLoS Comput. Biol.* **16**, e1007414 (2020).
59. J. M. Hondzinski, C. M. Soebbing, A. E. French, S. A. Winges, Different damping responses explain vertical endpoint error differences between visual conditions. *Exp. Brain Res.* **234**, 1575–1587 (2016).
60. C. Papaxanthis, T. Pozzo, J. McIntyre, Kinematic and dynamic processes for the control of pointing movements in humans revealed by short-term exposure to microgravity. *Neuroscience* **135**, 371–383 (2005).
61. S. Yamamoto, K. Kushiro, Direction-dependent differences in temporal kinematics for vertical prehension movements. *Exp. Brain Res.* **232**, 703–711 (2014).
62. C. Papaxanthis, V. Dubost, T. Pozzo, Similar planning strategies for whole-body and arm movements performed in the sagittal plane. *Neuroscience* **117**, 779–783 (2003).
63. E. Todorov, Optimality principles in sensorimotor control. *Nat. Neurosci.* **7**, 907–915 (2004).
64. J. K. Rilling, Human and nonhuman primate brains: Are they allometrically scaled versions of the same design? *Evol. Anthropol.* **15**, 65–77 (2006).
65. C. J. Donahue, M. F. Glasser, T. M. Preuss, J. K. Rilling, D. C. Van Essen, Quantitative assessment of prefrontal cortex in humans relative to nonhuman primates. *Proc. Natl. Acad. Sci. U.S.A.* **115**, E5183–E5192 (2018).
66. S. L. Hooper, C. Guschlbauer, M. Blumel, P. Rosenbaum, M. Gruhn, T. Akay, A. Buschges, Neural control of unloaded leg posture and of leg swing in stick insect, cockroach, and mouse differs from that in larger animals. *J. Neurosci.* **29**, 4109–4119 (2009).
67. S. L. Hooper, Body size and the neural control of movement. *Curr. Biol.* **22**, R318–R322 (2012).
68. A. von Twickel, C. Guschlbauer, S. L. Hooper, A. Büschges, Swing velocity profiles of small limbs can arise from transient passive torques of the antagonist muscle alone. *Curr. Biol.* **29**, 1–12.e7 (2019).
69. M. J. Wagner, J. Savall, T. H. Kim, M. J. Schnitzer, L. Luo, Skilled reaching tasks for head-fixed mice using a robotic manipulandum. *Nat. Protoc.* **15**, 1237–1254 (2020).
70. T. Schmidt, R. Lee, *Motor Control and Learning: A Behavioural Emphasis* (2005).
71. L. Shmuelof, J. W. Krakauer, P. Mazzoni, How is a motor skill learned? Change and invariance at the levels of task success and trajectory control. *J. Neurophysiol.* **108**, 578–594 (2012).
72. D. E. Angelaki, M. Q. McHenry, J. D. Dickman, S. D. Newlands, B. J. Hess, Computation of inertial motion: Neural strategies to resolve ambiguous otolith information. *J. Neurosci.* **19**, 316–327 (1999).
73. J. Laurens, H. Meng, D. E. Angelaki, Computation of linear acceleration through an internal model in the macaque cerebellum. *Nat. Neurosci.* **16**, 1701–1708 (2013).
74. L. C. Strotz, E. E. Saupe, J. Kimmig, B. S. Lieberman, Metabolic rates, climate and macroevolution: A case study using Neogene molluscs. *Proc. Biol. Sci.* **285**, 20181292 (2018).
75. J. H. Brown, J. F. Gillooly, A. P. Allen, V. M. Savage, G. B. West, *Ecology* (2004).
76. S. B. Munch, S. Salinas, Latitudinal variation in lifespan within species is explained by the metabolic theory of ecology. *Proc. Natl. Acad. Sci.* **106**, 13860–13864 (2009).
77. W. Van Voorhies, S. Ward, Genetic and environmental conditions that increase longevity in Caenorhabditis elegans decrease metabolic rate. *Proc. Natl. Acad. Sci. U.S.A.* **96**, 11399–11403 (1999).
78. J. P. DeLong, J. G. Okie, M. E. Moses, R. M. Sibly, J. H. Brown, Shifts in metabolic scaling, production, and efficiency across major evolutionary transitions of life. *Proc. Natl. Acad. Sci. U.S.A.* **107**, 12941–12945 (2010).
79. A. Berghänel, O. Schülke, J. Ostner, Locomotor play drives motor skill acquisition at the expense of growth: A life history trade-off. *Sci. Adv.* **1**, e1500451 (2015).
80. H. J. Huang, R. Kram, A. A. Ahmed, Reduction of metabolic cost during motor learning of arm reaching dynamics. *J. Neurosci.* **32**, 2182–2190 (2012).
81. P. Morel, P. Ulbrich, A. Gail, What makes a reach movement effortful? Physical effort discounting supports common minimization principles in decision making and motor control. *PLOS Biol.* **15**, e2001323 (2017).
82. W. Wang, N. Dounskaia, Load emphasizes muscle effort minimization during selection of arm movement direction. *J. Neuroeng. Rehabil.* **9**, 70 (2012).
83. B. Cheval, E. Tipura, N. Burra, J. Frossard, J. Chanal, D. Orsholits, R. Radel, M. P. Boisgontier, Avoiding sedentary behaviors requires more cortical resources than avoiding physical activity: An EEG study. *Neuropsychologia* **119**, 68–80 (2018).
84. R. Shadmehr, H. J. Huang, A. A. Ahmed, A representation of effort in decision-making and motor control. *Curr. Biol.* **26**, 1929–1934 (2016).
85. B. Pageaux, J. Gaveau, Studies using pharmacological blockade of muscle afferents provide new insights into the neurophysiology of perceived exertion. *J. Physiol.* **594**, 5049–5051 (2016).
86. D. W. Moran, A. B. Schwartz, Motor cortical representation of speed and direction during reaching. *J. Neurophysiol.* **82**, 2676–2692 (1999).
87. W. Wang, S. S. Chan, D. A. Heldman, D. W. Moran, Motor cortical representation of hand translation and rotation during reaching. *J. Neurosci.* **30**, 958–962 (2010).
88. R. C. Oldfield, The assessment and analysis of handedness: The Edinburgh inventory. *Neuropsychologia* **9**, 97–113 (1971).
89. E. Nakano, H. Imamizu, R. Osu, Y. Uno, H. Gomi, T. Yoshioka, M. Kawato, Quantitative examinations of internal representations for arm trajectory planning: Minimum commanded torque change model. *J. Neurophysiol.* **81**, 2140–2155 (1999).
90. B. Berret, E. Chiovetto, F. Nori, T. Pozzo, Evidence for composite cost functions in arm movement planning: An inverse optimal control approach. *PLOS Comput. Biol.* **7**, e1002183 (2011).

Acknowledgments: We thank D. Moran and T. Pearce for help in designing the monkey setup. **Funding:** The human work was supported by the Agence National de Recherche (ANR; project MOTION ANR-14-CE30-0007-01) and by the Centre National d'Etudes Spatiales (CNES), by the French "INVESTISSEMENTS D'AVENIR" program, project ISITE-BFC (contract ANR-15-IDEX-0003). The monkey work was supported by NIH grant R01-AT010459. **Author contributions:** J.G.: Conception and design, acquisition of data, analysis and interpretation of data, and drafting or revising the article; S.G.: Acquisition of data and drafting or revising the

article; B.B.: Analysis and interpretation of data and drafting or revising the article; D.E.A.: Conception and design, analysis and interpretation of data, and drafting or revising the article; C.P.: Conception and design, analysis and interpretation of data, and drafting or revising the article. **Competing interests:** The authors declare that they have no competing financial or nonfinancial interests. **Data and materials availability:** All data needed to evaluate the conclusions in the paper are present in the paper and/or the Supplementary Materials. Additional data related to this paper may be requested from the authors.

Submitted 18 November 2020
Accepted 19 February 2021
Published 7 April 2021
10.1126/sciadv.abf7800

Citation: J. Gaveau, S. Grospretre, B. Berret, D. E. Angelaki, C. Papaxanthis, A cross-species neural integration of gravity for motor optimization. *Sci. Adv.* **7**, eabf7800 (2021).